

# A simple measure of correlation across time, frequency and space between continuous brain signals

Jean-Philippe Lachaux<sup>a,\*</sup>, Mario Chavez<sup>a</sup>, Antoine Lutz<sup>a,b</sup>

<sup>a</sup> *Laboratoire de Neurosciences Cognitives et Imagerie Cérébrale (LENA), CNRS URA 654, Hôpital de La Salpêtrière, 47 Bd de l'Hôpital, 75651 Paris Cedex 13, France*

<sup>b</sup> *Department of Psychology, Laboratory for Affective Neuroscience, University of Wisconsin–Madison, 1202 West Johnson Street, Madison, WI, 53706, USA*

Received 27 August 2002; received in revised form 18 November 2002; accepted 19 November 2002

## Abstract

This paper introduces a simple but systematic method to estimate correlations between the spectral energy of two continuous electrophysiological signals in such a way that it can detect relationships between different frequencies and different latencies. From two series of signals (e.g. electroencephalogram, magnetoencephalogram or local field potentials) recorded from two sites in response to repeated sensory stimulations, the method computes the time–frequency energy of each signal. Then, it computes the Spearman rank order correlation coefficient across all the trials between the energy of the first signal series in one time–frequency region and the energy of the second signal series in a second time–frequency region. The method was designed to analyze interactions between frequency bands, in an effort to describe how the main brain rhythms interact with each other across time and space. It was applied to two simulations and to intracranial electro-encephalogram (EEG) recordings obtained from an epileptic patient performing two verbal discrimination tests (a phonological and a semantic task). It led to the identification of different correlations patterns in the gamma band depending on the level of semantic analysis performed by the patient.

© 2002 Elsevier Science B.V. All rights reserved.

**Keywords:** Time–frequency; Local field potential/electro-encephalogram/magneto-encephalogram; Inter-frequency correlations; Functional connectivity; Oscillations

## 1. Introduction

The method proposed in this paper stands at the intersection between two methodological lines of work in electrophysiology, the study of the so-called brain rhythms on the one hand, and the search for the large-scale interaction mechanisms that allow neural integration on the other hand. We propose a simple but systematic method to estimate cross-correlations between the spectral energy of two continuous electro-

physiological signals in such a way that it can detect relationships between different frequencies and different latencies.

Roughly speaking, electro-encephalogram (EEG) analysis techniques split into two major groups. A first line of techniques compute and analyze the average EEG signal obtained in response to repeated occurrences of the same experimental situation; for instance in response to repeated presentations of the same type of sensory stimulation. This is the classic evoked potentials (EP) averaging procedure designed to extract ‘evoked’ components that repeat themselves at the same latency and with the same phase for all the trials. Short components ( $\sim 20$  ms, for instance) cannot be detected by this procedure, unless they are very precisely time-locked to the stimulus (with a ms precision), this makes invisible virtually any activity above 30 Hz in the frequency spectrum, because the phase-dispersion of those components lead them to cancel out when they are

*Abbreviations:* TF, time–frequency; TFC, time–frequency correlation; TFROI, time–frequency region of interest; EEG, electro-encephalogram; MEG, magneto-encephalogram; LFP, local field potential; ERP, event-related potential.

\* Corresponding author. Tel.: +33-1-4216-1171; fax: +33-1-4216-1172.

*E-mail address:* [jean-philippe.lachaux@chups.jussieu.fr](mailto:jean-philippe.lachaux@chups.jussieu.fr) (J.-P. Lachaux).

averaged across the trials. A second line of techniques has been developed that extracts those components invisible for the EP procedure (termed ‘induced responses’, see Tallon-Baudry and Bertrand (1999) for a clear distinction). The simplest procedures are based on a computation of the power spectrum of the response signals to each individual stimulus, followed by the averaging of those spectra across the trials. This procedure detects frequency components that are not phase-locked to the stimulus, provided that they have enough power and last long enough relative to the duration of the spectral analysis window to count for sufficient power in the global spectrum. Such spectral analysis techniques have mostly been used to characterize the ubiquitous brain oscillations and their relationships to cognition (e.g. Hirai et al., 1999), (although the activity that those methods detect is often broadband and cannot really be termed ‘oscillatory’).

The characterization of brain oscillations in general has led to the well-known typology of ‘delta’ (1–4 Hz), ‘theta’ (4–7 Hz), ‘alpha’ (8–12 Hz), ‘beta’ (12–30 Hz) and ‘gamma’ (30 Hz and above) rhythms (further subcategorized according to their topography and cognitive correlates), that relates those frequency bands to certain brain states and cognitive processes (Basar et al., 2000).

Our understanding of brain oscillations have greatly benefited from the development of time–frequency transformation and time-scale decomposition techniques that can describe the temporal variations of the spectrum of non-stationary signals. Those methodological improvements have enabled the systematic studies of short oscillatory episodes (a couple of hundreds ms), such as gamma band induced responses, lasting 100–300 ms in the first 500 ms following the presentation of a sensory stimulus (e.g. Lachaux et al., 2000a,b).

The search for the functions of brain oscillations is livelier than ever (e.g. Tallon-Baudry and Bertrand, 1999; Kahana et al., 1999) and the repeated observations that those different brain rhythms can actually coexist (Raghavachari et al., 2001; Lutz et al., 2002) brings to still unexplored question of whether those rhythms interact with each other, to form complex distributed multi-frequency networks mediating the integration of multiple functions.

This question connects with another very active stream of research in brain imaging: the search for the neural mechanisms that allow distributed brain regions to interact with each other during unified coherent cognitive acts (Varela et al., 2001). While it is now clear that even simple cognitive functions involve large-scale neural networks, most of the results obtained with EEG/MEG/fMRI/TEP imaging techniques have described the components of those networks, without actually characterizing the interactions between them. A growing number of studies have acknowledged this limitation,

have formulated hypothesis on the neural interaction mechanisms and have developed analysis tools to detect those links (see Varela et al., 2001 for a review).

This research effort has focused on a search for statistical relationships between signals recorded simultaneously from various brain regions. With high-temporal resolution imaging techniques, such as EEG/MEG, most methodological efforts have analyzed specifically the relationships between the precise temporal organizations of brain signals. The most popular analysis tool so far to quantify those relationships has been coherence, which estimates the correlation between the frequency components of a signal in narrow frequency ranges (Gardner, 1992). Coherence has been used repeatedly to isolate short episodes of correlations between distributed neural components oscillating at the same frequency (Miltner et al., 1999). Using an alternative to coherence, that focuses solely on the phase-relationship between two oscillating signals (phase-locking statistics and single-trial phase-locking statistics) (Lachaux et al., 1999, 2002); we and others have described such ‘long-distance’ synchrony between brain structures separated by several centimeters, in relation to specific aspects of cognition (Rodriguez et al., 1999; Tallon-Baudry et al., 2001; Halgren et al., 2002).

More complex interaction mechanisms certainly coexist with synchrony, and it has recently been suggested that some phase-relationships may take place between neural components oscillating at different frequencies (Schanze and Eckhorn, 1997; Von Stein et al., 2000); which brings us back to the question of the relationships between the different brain rhythms.

So far, all the efforts in this direction have tried to characterize relationships between simultaneous brain signals. For instance, Von Stein et al. (2000) have used bicoherence to show a multi-frequency ‘synchrony’ in a behaving cat between gamma activity in area 17 and beta activity in area 7. To study EEG-EMG coupling in Parkinsonian patients, Tass and coworkers have introduced a procedure that detects  $n:m$  phase-locking, a situation in which an oscillator loops exactly  $n$  cycles while another one loops exactly  $m$  cycles (Tass et al., 1998). The question we address here is different and in a way, simpler, since we focus solely on energy emissions. To the exception of Friston (1997), we know of no systematic analysis technique that searches for correlations between the energy of two brain signals in two different frequency ranges. Friston (1997) proposed a method to test for the statistical dependence of the spectral densities measured from two sets of recordings in the same local time window. The method proposed in this paper tries to be more general in that it can quantify a statistical dependence between the energy of two signals in two different time–frequency regions. This means that it could quantify for instance the correlation, across trials, between the energy produced in one brain

region in the alpha band before the stimulation, and the energy produced in another brain region in the gamma band after the stimulation. It is a deliberate choice to focus on energy correlations and not phase relationships, since the notion of phase-locking makes little sense between non-simultaneous signals.

In contrast, we believe that the study of interactions between energies produced at different latencies can be very meaningful. We know for instance that the energy in the alpha band in ongoing EEG depends in some way on the vigilance level of an individual, we also know that the gamma activity induced by a stimulation depends on its attention level. The fact that there may be a correlation or anti-correlation between those two components is an interesting possibility that deserves to be tested. In fact, anti-correlation effects between alpha and gamma activity have already been reported in monkey V4 in a protocol manipulating visual attention (Fries et al., 2001).

In this paper, we introduce the present time–frequency correlation detector in detail and apply it to two simulations and to intra-cranial EEG recordings from an epileptic patient performing a visual verbal discrimination task.

## 2. Methods

### 2.1. Experimental data acquisition

The intracranial data presented in this paper were from a patient (one female) that suffered from an epilepsy resistant to all appropriate anticonvulsant medications. Electrodes were implanted in the left dominant hemisphere in order to localize the sites of seizure onset. The task was performed in the patient's hospital room, 4 days after the surgery, while she was waiting for spontaneous seizure onset. The patient had not had any complex partial seizure within at least the last 24 h, and her behavioral performance in the task was normal. The selection of the electrodes sites, mostly in the left temporal lobe, was made entirely on clinical grounds without any reference to the cognitive protocol. The participation of the patient in the cognitive protocol was made only after fully informed consent.

Electrodes were 0.8 mm in diameter and had ten recording contacts. Those contacts were 2 mm in length and regularly spaced every 3.5 mm. The recordings were monopolar with respect to a reference electrode in the white matter. Channels contaminated by frequent epileptiform abnormalities (spikes and bursts) were excluded from the analysis. Also, all the recording epochs showing epileptiform abnormalities were excluded.

The patient performed a series of visual language tasks. In the first condition shown in this paper (semantic task), the patient was presented with a series

of French words (5–6 letters) displayed on a computer screen in front of her, in foveal vision, and was asked to press a button with her right index finger when the word was the name of a living entity, or to press a second button with her right middle finger when it was not a living entity. Each word was shown for 2 s, and the interval between each word onset was chosen randomly between 2.8 and 3.2 s. The patient was presented with 260 words (50% of each kind). One hundred and fifty trials remained after a very careful artefact rejection procedure. In the second condition shown in this paper (phonologic task), the patient was shown with 5–6 letters pseudowords (words that can be pronounced in French, but that have no meaning). The presentation procedure was the same as above. The patient had to pronounce each pseudoword covertly in order to determine whether it ended like a consonant sound (like 'egg' in English) or a vowel sound (like 'marshmallow'). She responded with her right index finger in the former case and with her right middle finger in the latter case. Out of 260 pseudowords, 150 were kept for analysis after careful artefact rejection.

### 2.2. Data analysis

In the following, the method introduced in this paper will be referred to as time–frequency correlation, or TFC. Also, TF will refer to time–frequency. The TFC procedure is described in Fig. 1. Given two sets of signals  $x_i(t)$  and  $y_i(t)$ , corresponding to the signals recorded in response to a series of  $n$  events ( $i=1-n$ ) (sensory stimulations for instance) in two brain sites  $X$  and  $Y$ , the procedure follows two simple steps:

STEP A: compute the time–frequency transform of each signal in a frequency range of interest  $TF(x_i(t))$  and  $TF(y_i(t))$ , using a pseudo-smoothed Wigner–Ville transform or a short-term fourier transform then

STEP B: chose two time–frequency sub-regions of interest (TFROI), one for each brain site  $TFROI_X$  and  $TFROI_Y$ , and compute for each signal, the mean energy in the TF region chosen for its site. This yields two series of values  $m_{x_i} = \text{Mean}(TFROI_X)$  and  $m_{y_i} = \text{Mean}(TFROI_Y)$ , one series for each site, corresponding to the mean local TF energy of each event. The TFC is simply the Spearman rank correlation coefficient between those two series of values. This procedure is repeated for every possible choice of TFROI pair, and for each pair of recording sites. The total output of the procedure is thus 6-dimensional: time  $\times$  frequency  $\times$  time  $\times$  frequency  $\times$  channel  $\times$  channel.

Let's write this procedure in mathematical terms.

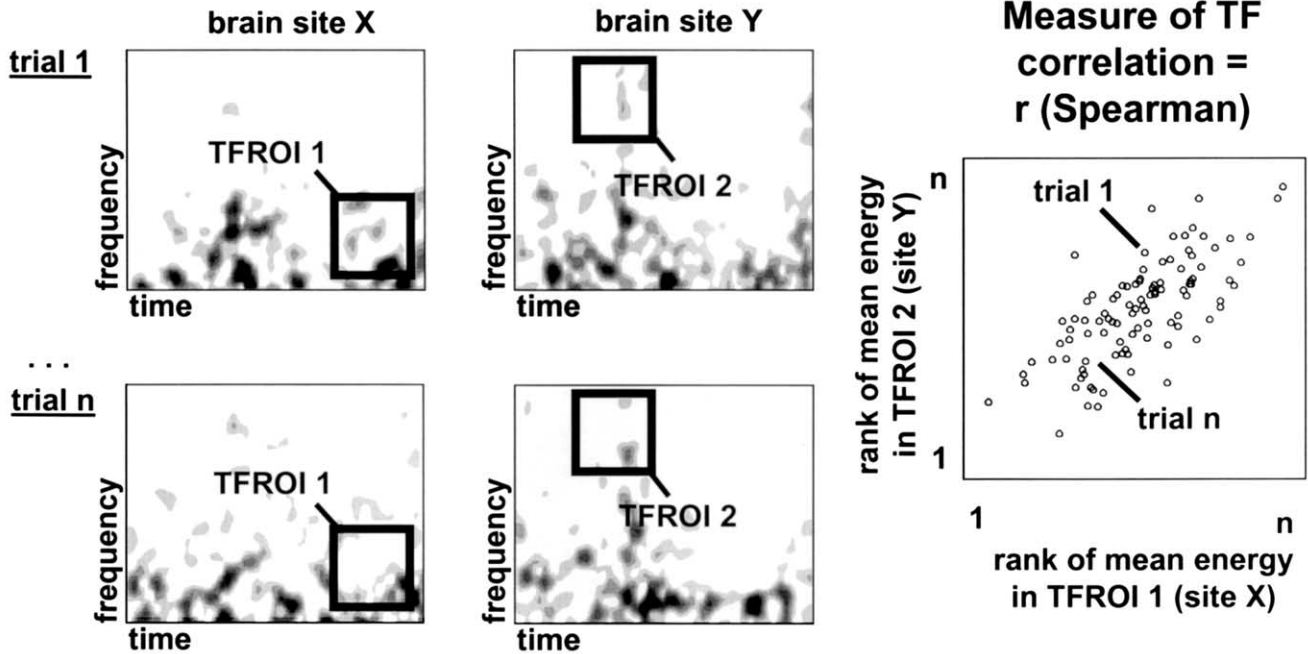


Fig. 1. Procedure used to compute the time–frequency correlation between two time–frequency regions of interest. Provided that for each trial (from 1 to  $n$ ), and for each recording site  $X$  and  $Y$ , the time–frequency transforms have been computed (four maps on the left: dark regions contain the highest energy), the user defines two regions of interest (one for  $X$  and one for  $Y$ ) in the time–frequency plane (TFROI1 and TFROI2). The average TF energy in each TFROI is computed for each trial, and those  $n$  values are ranked for each site from lowest to highest. Each trial is thus given two ranks, one for each site, and can be represented as a spot in a 2D plot (graph on the right). The time–frequency correlation between  $X$  and  $Y$  for this choice of TFROIs is the correlation coefficient between those two series of ranks.

The pseudo-smoothed Wigner–Ville transform of  $x_i(t)$  (resp.  $y_i(t)$ ) estimates the energy present in the signal around a time  $t$  and a frequency  $f$  as:

$$\text{PWV}(f, t) = \int_{-\infty}^{+\infty} |h(\tau/2)|^2 \left[ \int_{-\infty}^{+\infty} g(u-t)x_i(u+\tau/2)x_i^*(u-\tau/2)du \right] \cos(2\pi f\tau) d\tau$$

This formula is derived from the original definition of the Wigner–Ville transform to which two smoothing functions have been added (Auger et al., 1997):  $h$  is a short-term observation window used for frequency smoothing (in this study, a Hamming window of length 128 ms), and  $g$  is a temporal smoothing window (the same as  $h$  in this study). The purpose of these smoothing functions is to minimize interferences, a common limitation of the original Wigner–Ville transform (see Lachaux et al., 2000a,b for a discussion of the pseudo-smoothed Wigner–Ville transform applied to EEG signals).

Given a time–frequency region of interest  $[t_{\text{start}}:t_{\text{stop}}] \times [f_{\text{start}}:f_{\text{stop}}]$ , ranging from latencies  $t_{\text{start}}$  to  $t_{\text{stop}}$  and from frequencies  $f_{\text{start}}$  to  $f_{\text{stop}}$ . The average TF energy within that TFROI is simply:

$$Mx_i = \text{Mean}(\text{TF}(x_i(t)) \text{ on TFROI}_X)$$

$$= \frac{1}{(t_{\text{stop}} - t_{\text{start}})(f_{\text{stop}} - f_{\text{start}})} \cdot \int_{t=t_{\text{start}}}^{t=t_{\text{stop}}} \int_{f=f_{\text{start}}}^{f=f_{\text{stop}}} \text{PWV}(f, t) df dt$$

Those  $n$  values (one for each event) are then replaced by their rank within the series (yielding a new series  $Rx_i$ ), following the usual procedure used to compute the Spearman correlation coefficient. That is, if the smallest energy value is reached for trial 5 and the largest for trial 27, then we'll have  $Rx_5 = 1$  and  $Rx_{27} = n$ . The same procedure is performed with the series  $y_i$  and another TFROI to yield a rank series  $Ry_i$ .

Finally, the time–frequency correlation between  $x_i(t)$  and  $y_i(t)$  for that particular choice of TFROIs is the Spearman rank order coefficient:

$$r = 1 - \frac{6 \sum_i (Rx_i - Ry_i)^2}{n(n^2 - 1)}$$

It is a measure of monotonous association between the two series of values  $Rx_i$  and  $Ry_i$ . It is used to test two null-hypothesis that:

$H_0$ : ‘the mean energy measured in TFROI<sub>X</sub> in the signal recorded at site X does not progressively increase (resp. decrease) as the mean energy measured in TFROI<sub>Y</sub> in the signal recorded at site Y increases’.

The Spearman Correlation coefficient is preferred to the Pearson correlation coefficient for two reasons: first because the distributions of TF energy across the trials are not necessarily Gaussian, and second because it is more robust to the possible presence of very large energy values in some trials (that would be due to undetected artifacts for instance).

For large values of  $n$  (practically  $n > 30$ ), the distribution of that coefficient between two non-associated series (i.e. when  $H_0$  is true) can be approximated by a Gaussian distribution centered in zero and with a standard deviation equals to  $1/\sqrt{(n-1)}$ . For smaller values of  $n$ , significance tables are used. They quantify the probability that a certain value of  $r$  is reached without actually having any dependence between the series. This probability is obtained by comparing the estimated  $r$  with the distribution of all the possible  $r$  that can be computed between two series of  $n$  values (that is:  $n!$   $r$  coefficients obtained from  $n!$  possible pairs of rank series).

The size of the time–frequency regions of interest is to be adapted to the signals. In this paper, they extend over 500 ms in time and 5 Hz in frequency. Consecutive TFROIs overlap by 50% along either axis. It takes theoretically  $17 \times 14 = 238$  windows to cover the  $[-1000: +3000 \text{ ms}] \times [8-45 \text{ Hz}]$  time–frequency map:  $[-1000: -500 \text{ ms}] \times [8-13 \text{ Hz}]$ ;  $[-1000: -500 \text{ ms}] \times [10.5-15.5 \text{ Hz}]$ ;  $[-750: -250 \text{ ms}] \times [8-13 \text{ Hz}]$ , and so on... Practically, this decomposition can be slightly adapted to fit with the TF resolution of the TF maps, which is not always  $1 \text{ ms} \times 1 \text{ Hz}$ .

Because the global procedure measures one correlation coefficient for all possible pairs of TFROIs and all pairs of recording sites, the significance threshold must be adjusted to compensate for those multiple tests. To be on the safe side, the desired  $p$ -value  $p_{\text{desired}}$  should be divided by the total number of coefficients performed; that is, for 50 recording sites and 238 TFROI, as in the example above, one should chose  $p = 0.01/(50 \times 50 \times 238 \times 238) = 7 \times 10^{-11}$  for  $p_{\text{desired}}$  equal to 0.01 and compute the corresponding threshold  $r$ .

One particularity of the proposed method is that it can be seen as a natural extension of the classic procedure used to compute the average time–frequency energy emitted in a brain site in response to a series of events. It parallels the way this averaging procedure was itself a natural extension of the procedure used to compute the average frequency distribution of the energy emitted in response to repeated events (see Fig. 2). Before time–frequency analysis was applied, the presence of oscillatory components in the response to

stimulations was detected by computing the power-spectrum of each  $x_i(t)$  and by averaging those across the trials (using the same notations as above). This method did not allow to make the important distinction between the two scenarios illustrated in Fig. 2: scenario 1 (resp. scenario 2) in which high-frequency components arise before (resp. after) low–frequency components. Time–frequency analysis resolve such ambiguities, it describes the response’s structure not just along the frequency dimension but also along the time dimension. In the same way, it is not possible, by simply computing the average time–frequency energy maps across the trials, to distinguish between scenarios 3 and 4. In both scenarios, high-frequency components arise after the low-frequency components. Yet, in scenario 4, both components covary in amplitude from trial to trial, as if they were part of a single, complex response that spans over multiple latencies and frequencies, while in scenario 3, the low and high-frequency components seem independent of each other as if they corresponds to two separate responses. The two mean time–frequency maps, averaged across trials are identical in both scenarios. But the measure of TFC between those two TFROIs allows one to distinguish between the two situations; it now provides an insight into the response’s structure along the ‘events’ dimension.

TFC visualization: Fig. 3 describes a convenient procedure to visualize the 6-dimensional data produced by the algorithm. A two-steps visualization permits to capture the structure of the results along all three axis time, frequency and channel.

### 3. Results

#### 3.1. Simulations

The TFC coefficient was applied to two simulated sets of data.

In the first simulation (S1), the data simulated recordings from two brain sites in response to 50 consecutive presentations of the same sensory stimulation. In the first site, a strong ongoing alpha rhythm ([8–12 Hz]) stopped at the stimulus onset, while in the second site, the stimulation induced a strong gamma response ([30:40 Hz]) after 500 ms. The stronger the alpha rhythm in the first site, the weaker the gamma response in the second site, as if the amplitude of the gamma response was correlated with the vigilance level of the (simulated) individual before the stimulation, and if the amplitude of the ongoing alpha was a (anti-)marker of that vigilance level (strongest alpha levels would correspond to the least vigilant states).

In the second simulation (S2), the data correspond to the signals recorded in a single brain site in response to 50 consecutive identical sensory stimulations. The

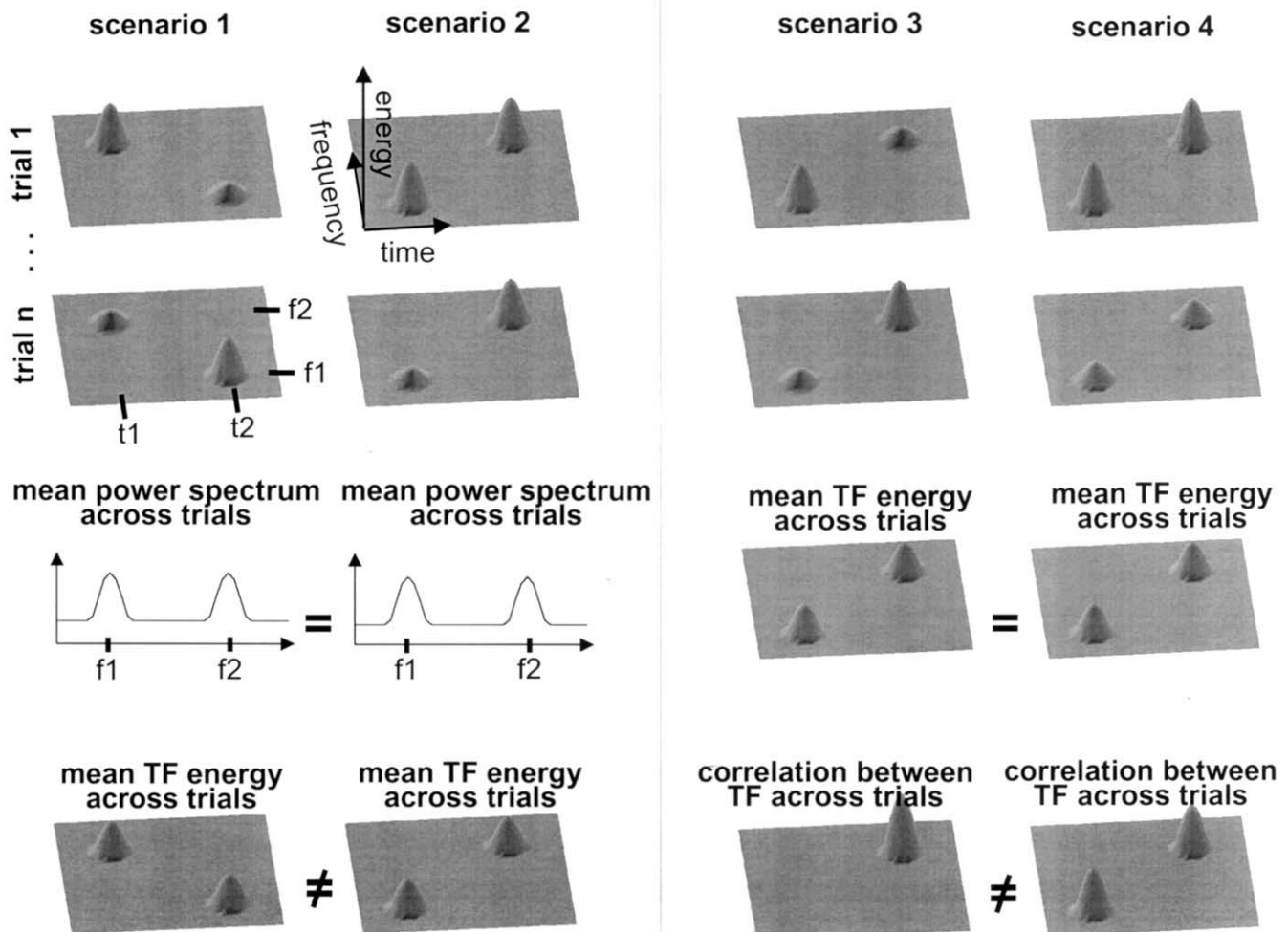


Fig. 2. A closer look into the time–frequency structure of EEG signals. This figure depicts four different scenarios. In the first two scenarios, consecutive stimuli generate a neural response in two frequency ranges ( $f_1$  and  $f_2$ ), a high-frequency response at time  $t_1$  followed by a low-frequency response at  $t_2$  in scenario 1, and the reverse in scenario 2 (top TF maps). It is not possible to distinguish between those two scenarios by simply calculating the average power-spectrum of the responses across the trials (middle). However, the average TF map across the trials is not the same for scenario 1 and 2; it describes the organization of the response in time. In the last two scenarios, consecutive stimuli generate a neural response in the same TF regions, but with amplitudes that covary (scenario 4) or not (scenario 3) from trial to trial (top TF maps). While such a covariation can be the sign that the two components are part of the same complex response components, it cannot be detected by simply averaging the TF maps across trials. The mean TF maps are identical for scenario 3 and 4 (middle maps). The bottom maps show the TF correlation between every TFROI and the TFROI centered in  $(t_2, f_2)$ . The two scenarios yield two different correlation maps: the TFC reveals an important aspect of the organization of the responses across the trials.

stimulation induce a complex response made of an early ([0:1000 ms]) component in the beta range ([20:25 Hz]), and a late ([1750: 2750 ms]) component in the gamma range ([40:45 Hz]). The amplitude of those two components covary from trial to trial and really act as one multi-frequency block.

Both simulations are described in detail in [Appendix A](#).

The results are shown in [Fig. 4 \(S1\)](#) and [Fig. 5 \(S2\)](#). The TFC was computed each time between one TFROI covering one of the response components, and all the other TFROIs including those covering the other active component. In S1, the reference TFROI corresponded to the induced gamma response of the second site, which

correlated negatively ( $p_{\text{desired}} < 0.01$ ) with the ongoing alpha of the first site. In S2, the reference TFROI corresponded to the induced beta response and it was positively correlated ( $p_{\text{desired}} < 0.01$ ) with the induced gamma response.

### 3.2. Intra-cranial EEG data

To illustrate the method, we selected one recording site located in the cingulate parietal gyrus and computed the TFC between all possible pairs of TFROI on the time–frequency interval  $[-1000 \text{ ms}: 3000 \text{ ms}] \times [8 \text{ Hz}: 45 \text{ Hz}]$  (words and pseudowords appeared at 0 ms). TFROIs were  $[500 \text{ ms} \times 5 \text{ Hz}]$ ; there was a 250 ms (50%)

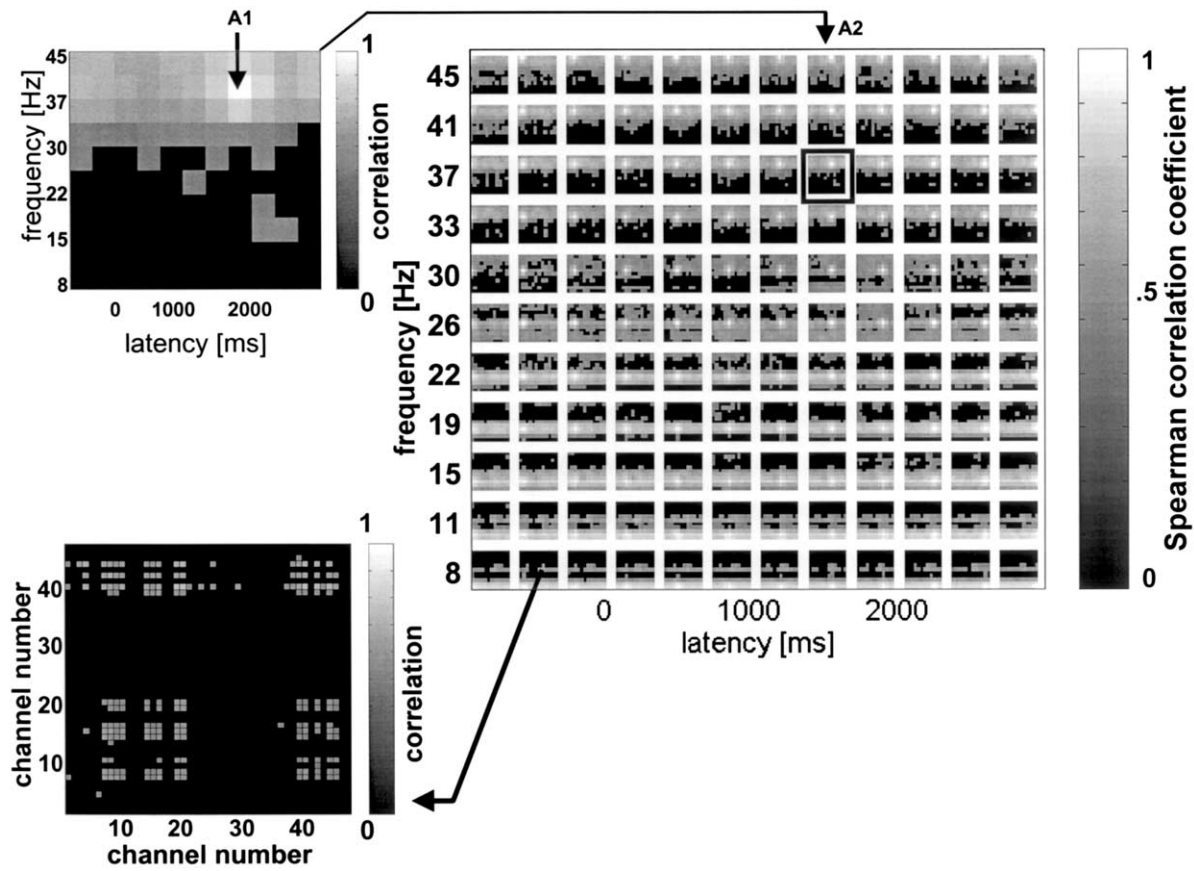


Fig. 3. TFC visualization. How to display a 6-dimensional object? For a given TFROI, (chosen as reference and noted TFROI<sub>r</sub>), the procedure produces one correlation coefficient with all the other TFROIs, for each pair of recording site. The maximum coefficient across all pairs is just one number that can be displayed for each TFROI on a TF display (top left matrix) (Note that coefficients that are not significant are set to zero, to simplify the visualization). The matrix value is obviously 1 in TFROI<sub>r</sub>, which allows one to identify this reference region clearly, with a white dot (arrow A1). The matrix displays thus the maximal correlation between this 'white dot' region and all the other ones in the TF plane. It can be inserted into a larger matrix (to the right: arrow A2) that contains all the other matrices obtained in the same way for all the other TFROIs taken themselves as references. The TF location of a small matrix into the larger one is a function of its TFROI (black frame), it is identified by its latency and its frequency [nested axis]. The channel by channel description, which is lost in the large matrix that only displays the maxima, can be recovered in our simple visualization program: clicking on any element of the large matrix produces a display of the correlation coefficients, for that element, between all the channels (bottom left). (Note that in the large right matrix, white vertical and horizontal stripes are just for separation purposes.)

overlap along the time axis and a 3 Hz (60%) overlap along the frequency axis. A total of 204 (12 × 17) TFROIs were defined that way.

Fig. 6 shows the average time–frequency energy maps across the trials in response to words and pseudowords. Both maps display the classic monotonic decrease with the frequency, but the profile along the time axis is quite different between the two conditions, this can be clearly seen at low frequencies. Also, in the response to words, there is a ripple of energy around 35 Hz that lasts for the whole window. There is no way to tell from the average map whether this ripple is the trace of a continuous stream of energy at this frequency, that would last during the full duration of each trial, or whether it corresponds to the accumulation of energy bursts appearing at random latencies from trial to trial.

The TFC calculation supports the first scenario. At the highest frequencies (roughly above 20–25 Hz, in the

beta-gamma bands), there is a significant correlation between all the TFROIs. This means that the gamma activity at this recording site behaves as a continuous stream, with an amplitude that varies little between the beginning of a trial and the end of it. In contrast, at the lower frequencies, the correlation drops sharply below the significance level as the time separation between two TFROIs exceeds 500 ms. This means that the lower frequencies are due to isolated bursts of energy.

Interestingly, the amplitude of those effects depends on the experimental condition. Figs. 7 and 8 shows two TFC maps extracted (zoomed in) from the global matrix of Fig. 6. The first zoom (Fig. 7) shows the TFC between all the TFROIs and the TFROI centered in [1250 ms × 34 Hz]. The variations of the TFC along the time axis, at 34 Hz, illustrate the continuity of the gamma activity. The correlation remained significant over the whole time interval. However the TFC decrease

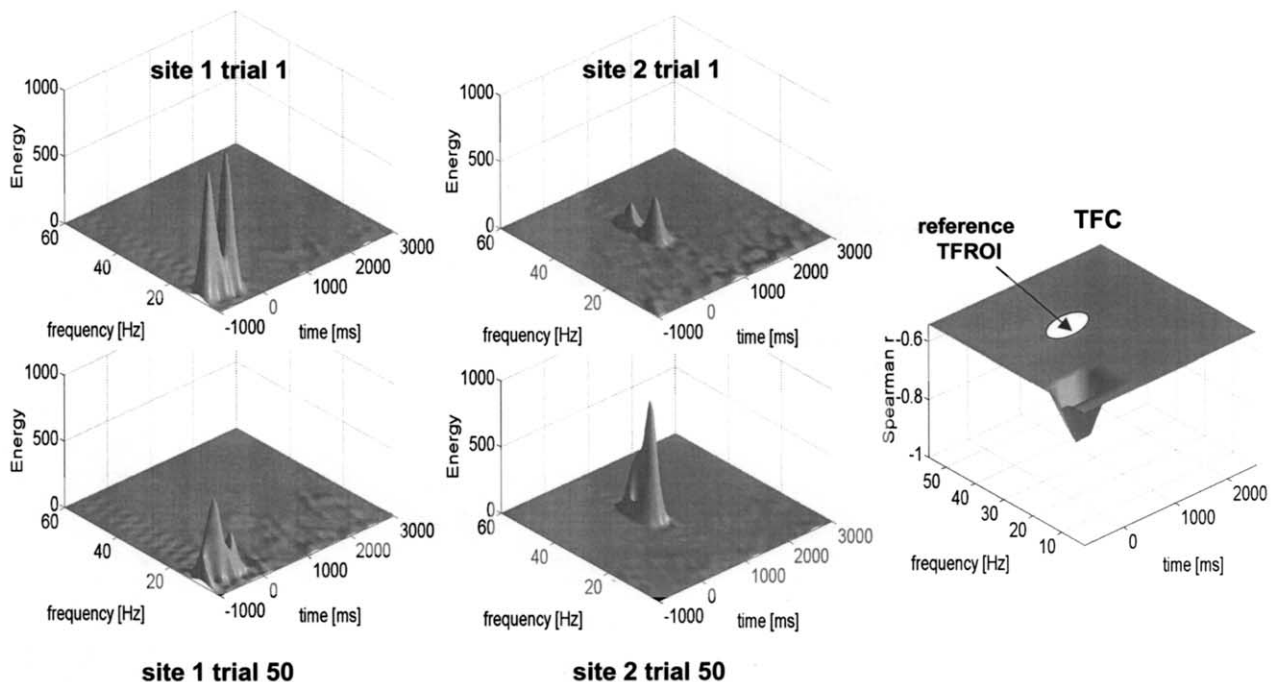


Fig. 4. First simulation: anti-correlation between the ongoing alpha in one recording site, and an induced gamma response in a second site. The four graphs on the left show for each site the TF energy maps for two trials (1 and 50). When the pre stimulus energy goes down in the alpha band in the first site, the post-stimulus energy goes up in the gamma band in the second site. The fifth graph on the right shows the significant TFC obtained between the reference TFROI centered in the gamma induced response of the second site (white circle) and all the other TFROIs measured in the first signal. There is a significant negative correlation between the energy of the ongoing alpha in the first site and the energy of the induced gamma response in the second site.

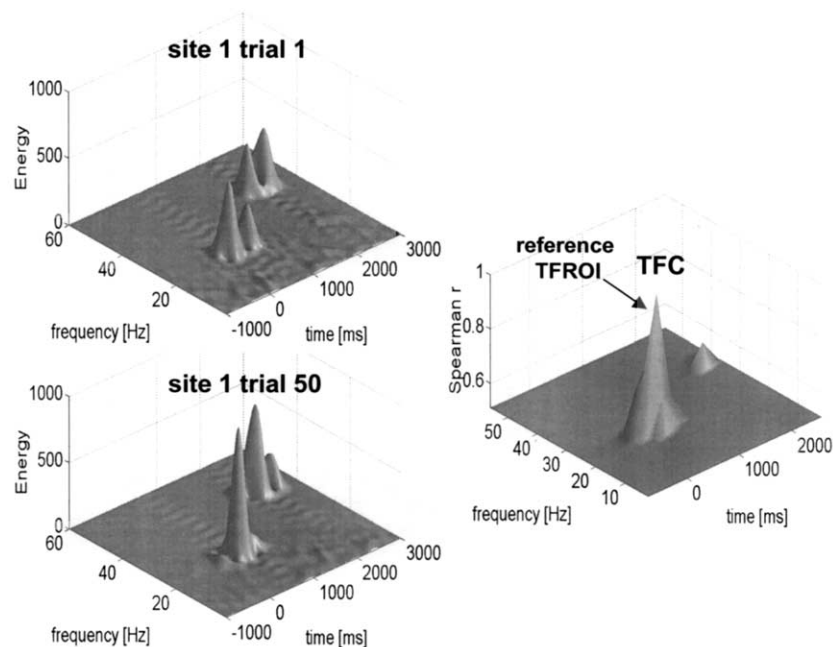


Fig. 5. Second simulation: correlation between early beta and late gamma components of the induced response. The two graphs on the left show the TF energy maps for two trials (1 and 50). When the post-stimulus energy goes up in the beta band it also goes up in the gamma band a couple of hundreds milliseconds later. The third graph on the right shows the significant TFCs obtained between the reference TFROI centered in the early beta induced response and all the other TFROIs. There is a significant positive correlation between the energy of the induced beta response and the energy of the induced gamma response.

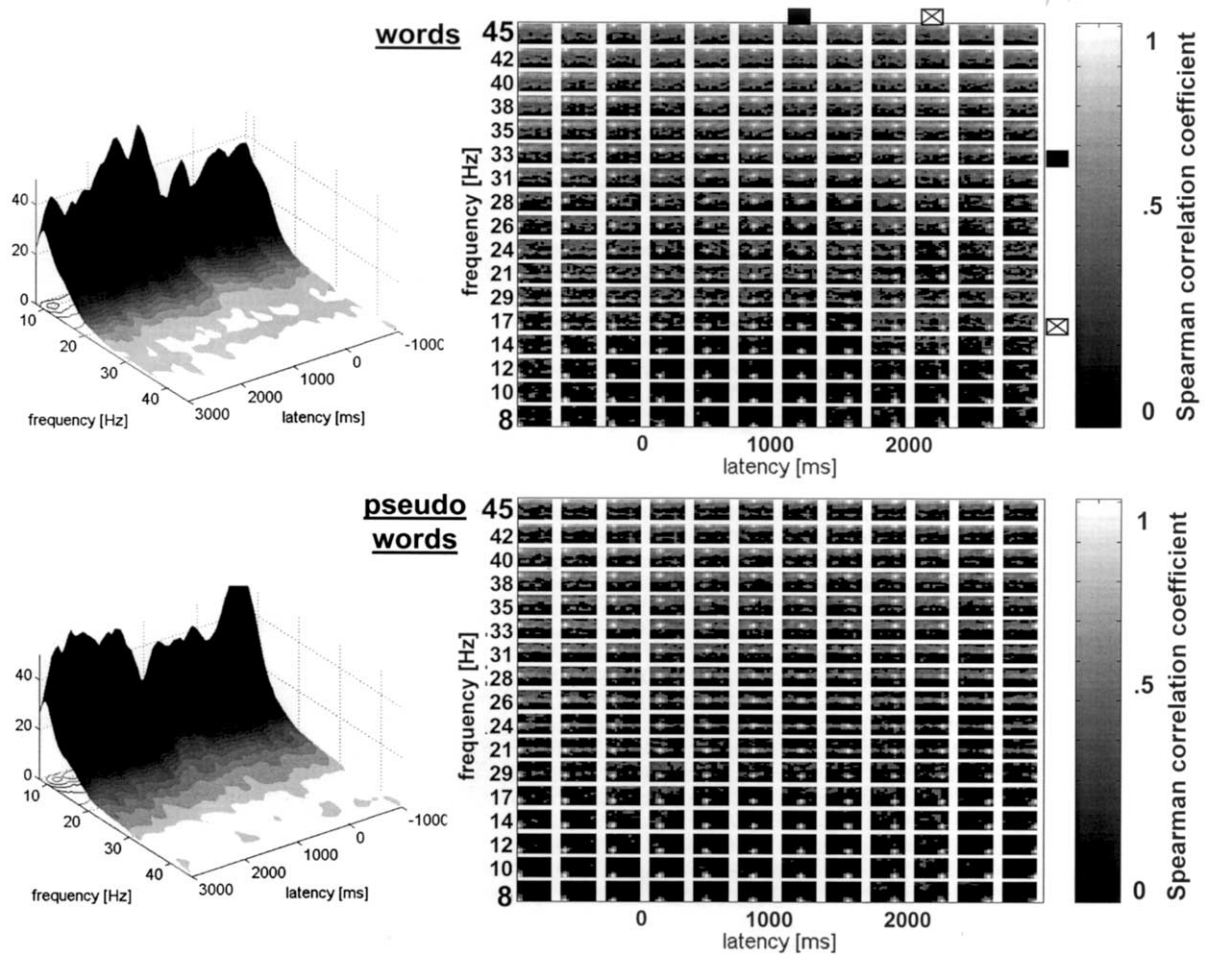


Fig. 6. TFC and mean TF energy maps in response to words and pseudowords. Left graphs show the mean of the pseudo-smoothed Wigner–Ville transform of 150 signals recorded in the cingulate parietal gyrus in response to words (top) and pseudowords (bottom). Time goes from right to left so that small energy high-frequency components are visible. Character strings appeared at 0 ms and lasted for 2000 ms, followed by a small fixation point. Right graphs show the TFC between all pairs of TFROIs in the way described in Fig. 3, in each large matrix, the location of a TFROI is determined by its latency and frequency [nested axis]. TFC were set to 0 if not significant. The Spearman  $r$  significance level for the TFC was 0.4, for a  $p$ -value of 0.01 corrected for multiple tests. The black and crossed squares indicate two TFROIs further described in the subsequent figures. See text for a discussion of those results.

was much sharper in response to pseudowords than words, as if the gamma stream was more continuous in the semantic task. The TFC variations along the frequency axis also had different profiles in the two conditions. In response to words, the TFC decrease with frequency separation was less sharp, as if the semantic processing involved a broader frequency component than the phonologic processing.

Similar effects were observed for a slower and later TFROI [2500 ms  $\times$  17 Hz] (Fig. 8). The TF energy components were broader along both axis in response to words. In response to pseudowords, the TFC were not significant beyond a [1000 ms  $\times$  5 Hz] separation, while it was almost always significant in response to words.

Such differences between the TFC in the two conditions are potentially important clues about the neural dynamics of the region explored. Since in the experi-

mental protocol, words and pseudowords were presented in different blocks, it is reasonable to assume that the patient developed a separate cognitive strategy for each stimulus type that it engaged at the beginning of each block for its entire duration. The high TFC values in response to words during semantic processing may therefore reveal the fact that such long-term strategies are mediated by continuous neural activations in specific frequency ranges.

#### 4. Discussion

The results presented above demonstrate that the proposed method is well suited to detect correlations between the energy of two signal components of possibly different frequency, occurring at different latencies relative to a repeated stimulus. Applications

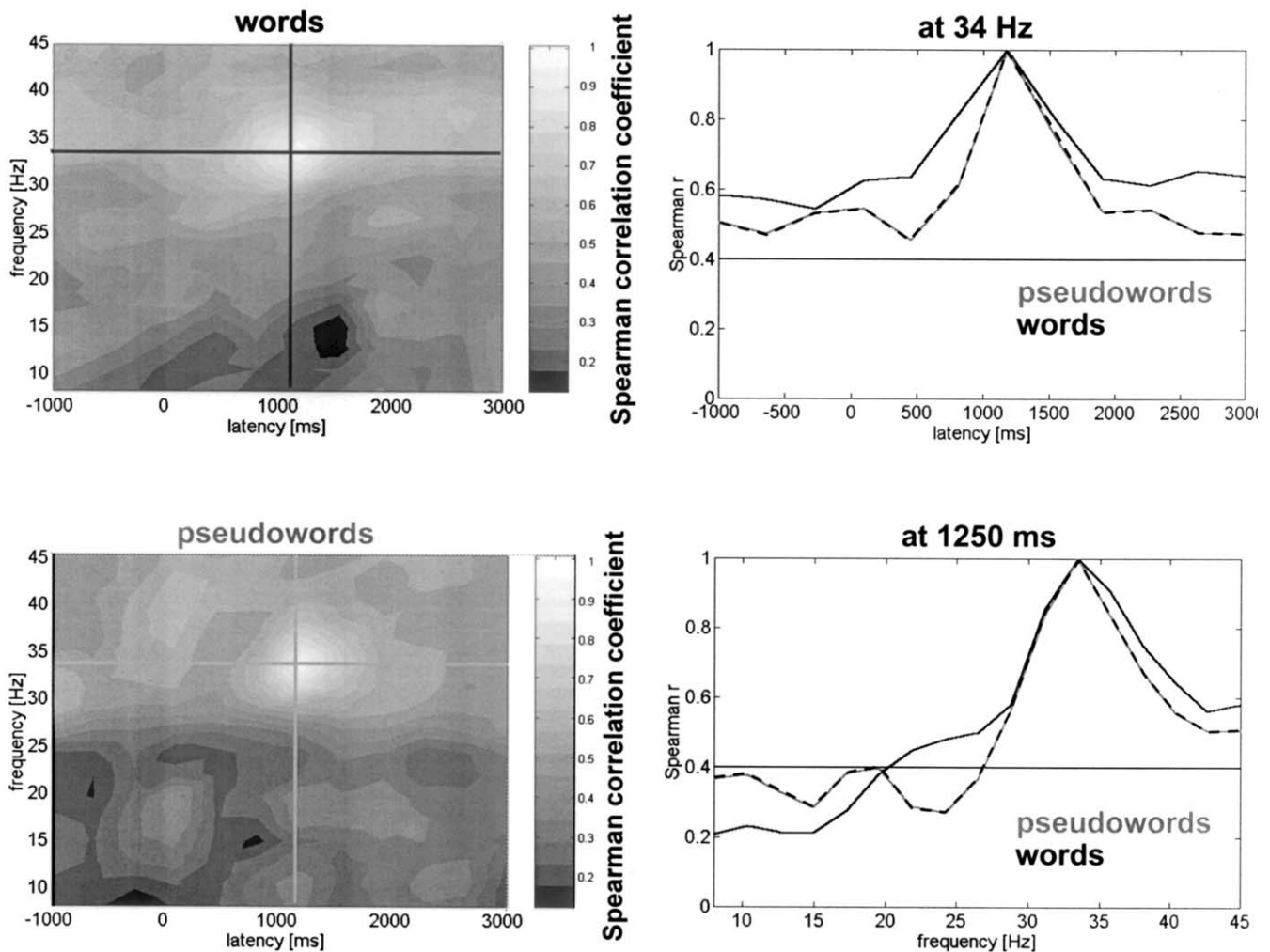


Fig. 7. TFC between the TFROI centered at (1250 ms  $\times$  34 Hz) and all the other TFROIs. Left maps have been zoomed in from the right matrix in Fig. 6 (row and column marked by a black square) and display the raw TFC for words (top) and pseudowords (bottom) (both significant and non-significant values are shown). Right: top graph shows a horizontal slice of the left maps along the line at 34 Hz for words (black) and pseudowords (dashed-gray). Significance level was at 0.4 as in Fig. 6. Bottom graphs show a vertical slice of the left maps along the line at 1250 ms for words (black) and pseudowords (dashed-gray).

of this method include: (a) the detection of significant correlations between the energy emitted in one frequency range in one brain region before the occurrence of a stimulus and the energy emission in another frequency range after the stimulus in another, or in the same, brain region; (b) the measure of the correlation between two frequency components occurring at the same time in one brain region, to test whether they belong to the same global large-band component that repeats across the trials, or whether they correspond to two independent processes.

#### 4.1. Practical aspects

The principle and implementation of the method is fairly simple, once the time–frequency transforms of the signals have been computed using standard routines. Yet, one may be concerned by the fact that this analysis

produces 6-dimensional results (channel  $\times$  channel  $\times$  time  $\times$  frequency  $\times$  time  $\times$  frequency). The trend in EEG data analysis is to produce results of increasing dimensionality. Evoked potentials are 2 dimensional objects (time  $\times$  channel), mean time–frequency power maps are 3-dimensional (time  $\times$  frequency  $\times$  channel) and coherence and mean synchrony measures are 4-dimensional (time  $\times$  frequency  $\times$  channel  $\times$  channel). The risk when increasing dimensionality is to end up with results that are simply unmanageable: impossibly long to compute and to browse through. Fortunately, the computation requirements of this method are fairly reasonable. For instance, working directly on the time–frequency maps already computed for all the trials and electrodes, it took 30 min to our Matlab<sup>®</sup> algorithm to analyze intracranial EEG data such as those presented above for 40 recording sites on a 800 MHz PC with 256 Mb of RAM.

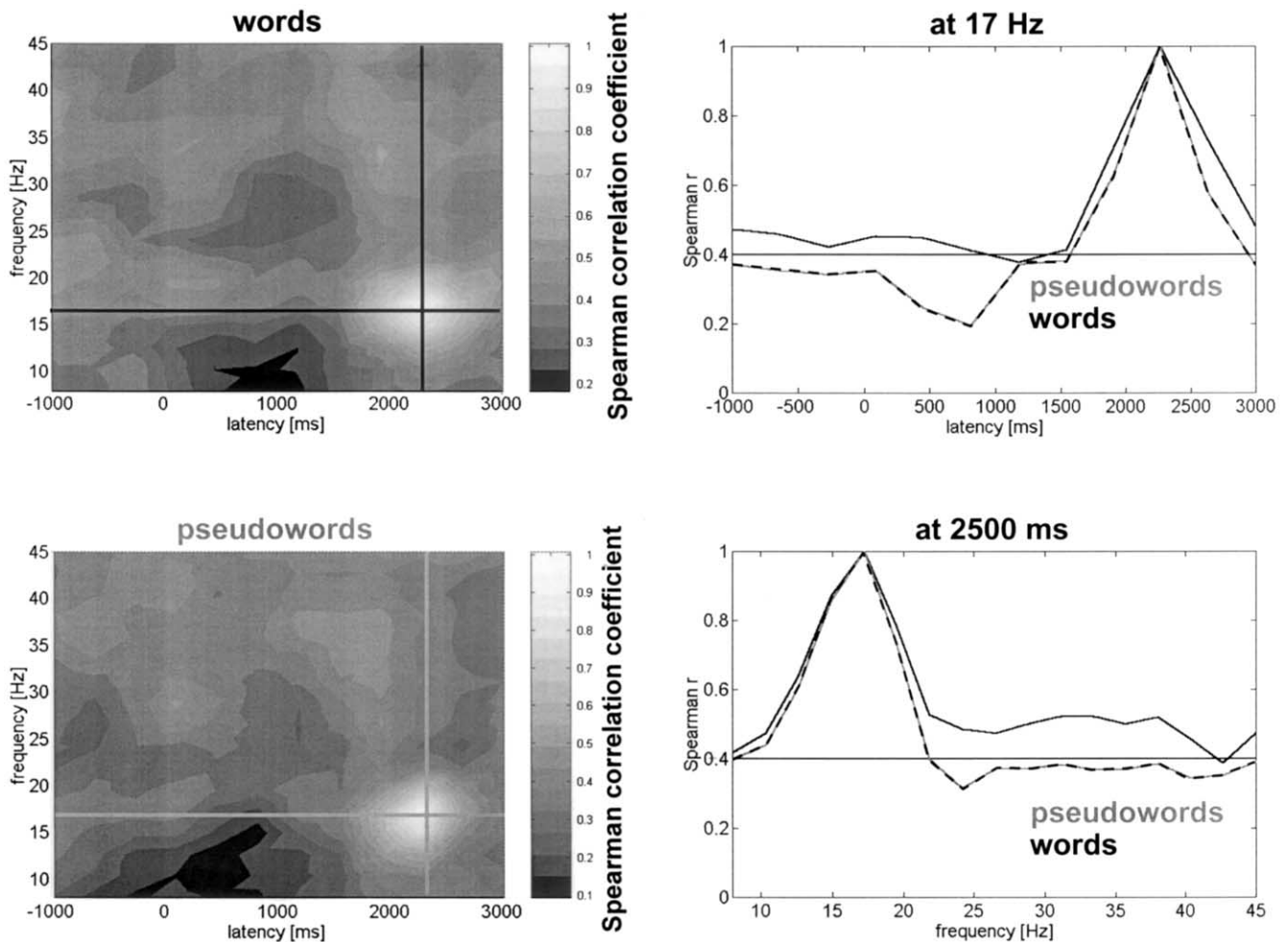


Fig. 8. TFC between the TFROI centered at (2500 ms  $\times$  17 Hz) and all the other TFROIs. Left maps have been zoomed in from the right matrix in Fig. 6 (row and column marked by a crossed square) and display the raw TFC for words (top) and pseudowords (bottom) (both significant and non-significant values are shown). Right: top graph shows a horizontal slice of the left maps along the line at 17 Hz for words (black) and pseudowords (dashed-gray). Significance level was at 0.4 as in Fig. 6. Bottom graphs show a vertical slice of the left maps along the line at 2500 ms for words (black) and pseudowords (dashed-gray).

Browsing through the data is greatly facilitated by the fact that most correlation coefficients are non-significant. The systematic exploration of the remaining significant coefficients is performed using procedure described in Fig. 3. We found this procedure to be a convenient alternative to the hassle of finding a way to display 6 dimensions in one shot.

From an EEG signal analysis point of view, the present method generalizes on the extraction of neural transients described by Friston (1997). His analysis is somewhat equivalent to the correlation measure we propose, when it is computed between simultaneous time segments of two sets of time–frequency maps (that is, on the results map on the left graphs of Figs. 7 and 8, they would correspond to the coefficients in the vertical band containing the reference time–frequency tile). The method we introduce also detects dependence between non-simultaneous signals.

In fact, it is a very natural extension of the averaging procedure used to compute induced spectral responses, such as the induced gamma response. While that averaging procedure computes the mean distribution of energy in the TF plane for one recording site across the trials, the present method estimates the conditional distribution of energy in the TF plane for one recording site, given the distribution of energy for a second recording site. In a sense, this is similar in spirit to the natural step that leads one from the computation of post-stimulus spike histograms (the probability for a neuron to spike at each latency relative to a stimulus) to the cross-correlogram (the probability for a neuron to spike at a given latency, given the spike train of another neuron). We move from a first-order probability distribution to second-order conditional probability distributions. The present method can in fact be modified in a minor way to produce an exact analog of the spike

cross-correlogram: for this, the correlation must be computed between binarized TF maps, that identify TF bursts of energy in single trials (following the binarization procedure proposed in Lachaux et al., 2000a,b, for instance).

#### 4.2. Relevance for the study of LFP/EEG/MEG signals

This method brings new information about the structure of EEG that was inaccessible via traditional averaging procedure. For instance, Raghavachari et al. (2001) have shown examples of averaged TF maps obtained in multiple intra-cranial brain regions during memory tasks, which showed two clear simultaneous components in the theta band and in the alpha band. It was not mentioned whether those components occurred independently of each other or whether they belonged to a single bi-band component. In the first scenario, our method should detect no cross-band correlation at the time of the induced response, while in the second scenario, it should detect one, since the large-band component would vary as one block from trial to trial.

Since the proposed method also quantifies the temporal correlation in each frequency band, it should detect temporal patterns that act as ‘solid’ blocks such as systematic, frequency-specific, energy undulations. Since the correlation is also computed between distinct channels, this provides an opportunity to observe how the emergence of a frequency component in one brain structure correlates with the increase or decrease of energy later in other brain structures, in another part of the spectrum. The present method is one possible approach to probe the effect of ongoing activity on the neural response to a stimulus.

Our correlation measure is ideally-suited for signals with high signal-to-noise ratio, such as human intra-cranial recordings or, even better, LFPs measured in animals. In those signals, oscillations are often seen with the naked-eye in single trials. The situation is different with more global recordings such as MEG and EEG, in which the signal of one electrode averages the activity of vast populations of cells. In such cases, local oscillations may be hard to extract from the background neural activity that is generally non-oscillatory. This can potentially limit the application of the TFC calculation, not because of the method, but because of the signals themselves. Still, some low frequency rhythms (i.e. alpha) are very visible in such global signals, and at higher frequencies, one can often observe broadband stimulus-related increases of energy (Tallon-Baudry and Bertrand, 1999, 1); so, since those components can be extracted from the signals, the TFC calculation is legitimate, although it may be wise to use more trials than with signals with higher signal-to-noise ratio. Another general concern is that the reference electrode may add a common noise that could potentially increase

the correlation level spuriously, in which case the TFC would tell more about the structure of the reference signal than about the structure of neural activity. This is especially true for EEG signals, since with intracranial recordings, it is always possible to use bipolar recordings or very silent reference electrodes. This reference issue is not specific of the TFC method, but is a recurrent concern of every EEG-based analysis. As a rule of thumb, one could use the fact that the same spurious correlations should be found between every pair of electrode, and within every electrode; therefore, TFC measures that are specific of certain electrode pairs are unlikely to be due to reference contamination. Another possibility is to apply the TFC measure on de-referenced data such as Laplacian-transformed EEG.

#### 4.3. Limitation and further improvements

The present method was designed as a first and simple approach to probe energy relationships through time, space and frequency. It suffers some limitations due to its simplicity. The main one is that it computes a linear correlation, and as such, it does not allow one for instance to conclude that one TF pattern is having a direct driving effect on another one. Also, it can be blind to most forms of non-linear relationships. This is a general limitation of the classic correlation coefficient, and the simple principle of the method can be applied with other correlation measures that are better-suited for specific types of non-linearity. Possible remedies may involve higher-order statistics such as Volterra series (Friston, 2000) (approaches currently explored in our group).

Also, the method only measures correlations between energy variations. Other relevant parameters can be used to describe TF components, such as the latency or the frequency at which a given pattern occurs. One may imagine that the energy in the alpha band prior to the stimulation may correlate with the latency of gamma induced responses. Along this idea, Bressler (2002) have shown in the LFP of monkeys performing a go–nogo task, the latency of the N100 evoked over parieto-occipital areas by the visual stimulus was shorter when the power in the frontal beta activity was higher.

The analysis presented in this paper is open to a possibly useful modification, in which the correlation between TF energy would not be measured across trials but in time. This would be used to detect correlations between the simultaneous temporal variations of TF energy in two frequency ranges, when one has only one long continuous recording, instead of multiple trials. Practically, the analysis would be the same, except that for each recording site, the population of TF energy values used to compute the correlation coefficient would not correspond to the energy in a single TFROI for

successive trials, but to the energy in consecutive TFROIs of the single continuous recording.

Finally, the present method cannot address a third type of interactions between frequency components: those involving phase-relationships. As previously mentioned, the investigation of phase-relationships was deliberately left aside in this paper, and methods like the bicoherence specifically address this point. Still, it may be of interest to develop in parallel methods that can test whether the energy or the latency of a frequency component induced by the stimulus depends in some way of the value of the phase (of a second signal at a second frequency) when the stimulus occurs.

Despite those limitations, the possibilities of such a simple method are promising ones. As it is completed by other analysis techniques that can probe systematic linear and non-relationships between the latencies, frequencies and phase of EEG signal components, while providing manageable results, we should go way past the understanding gained with classic ERP analysis and move towards a true description of the brain dynamics.

## Acknowledgements

The authors are especially grateful to P. Kahane, M. Le Van Quyen, J. Martinerie and D. Rudrauf for useful discussions.

## Appendix A

In the first simulation S1, the system was the following,  $Y_{1,\text{trial}}(t)$  and  $Y_{2,\text{trial}}(t)$  the signals for a trial and for the first and the second site were defined by:

$$Y_{1,\text{trial}}(t) = X_{1,\text{trial}}(t) + C_{1,\text{trial}}X_{1,\text{trial}}^a(t)$$

and

$$Y_{2,\text{trial}}(t) = X_{2,\text{trial}}(t) + C_{2,\text{trial}}X_{2,\text{trial}}^g(t)$$

where  $X_{1,\text{trial}}(t)$  and  $X_{2,\text{trial}}(t)$  were actual signals recorded from the patient described above (the signals were different for each trial).

$C_{1,\text{trial}}$  and  $C_{2,\text{trial}}$  were numbers chosen randomly for each trial between 500 and 1500 from a uniform distribution, such that  $C_{1,\text{trial}} + C_{2,\text{trial}} = 1000$ , always.

$$X_{1,\text{trial}}^a(t) = \frac{X'_{1,\text{trial}}{}^a(t)}{\|X'_{1,\text{trial}}{}^a(t)\|}$$

with  $X'_{1,\text{trial}}{}^a(t) = A(t)\text{Fil}_{8-12 \text{ Hz}}(X_{1,\text{trial}})$ . ( $\|U(t)\|$  is the norm of  $U(t)$ ).

$A(t)$  was a function that was zero everywhere except on the window  $[-1000-0 \text{ ms}]$  where it decreased continuously from 1 to 0.

$\text{Fil}_{8-12 \text{ Hz}}(X_{1,\text{trial}})$  was signal  $X_{1,\text{trial}}(t)$  bandpass-filtered between 8 and 12 Hz.

$$X_{2,\text{trial}}^g(t) = \frac{X'_{2,\text{trial}}{}^g(t)}{\|X'_{2,\text{trial}}{}^g(t)\|}$$

with  $X'_{2,\text{trial}}{}^g(t) = G(t)\text{Fil}_{30-40 \text{ Hz}}(X_{2,\text{trial}})$ .

$G(t)$  was a function that was zero everywhere except on the window  $[0-1000 \text{ ms}]$  where it was a bell curve, with a maximum value equal to 1.

$\text{Fil}_{30-40 \text{ Hz}}(X_{2,\text{trial}})$  was signal  $X_{2,\text{trial}}(t)$  bandpass-filtered between 30 and 40 Hz.

In the second simulation S2, the system was the following,  $Y_{\text{trial}}(t)$  the signal for a trial was defined by:

$$Y_{\text{trial}}(t) = X_{\text{trial}}(t) + C_{\text{trial}}(X_{\text{trial}}^g(t) + X_{\text{trial}}^b(t))$$

where  $X_{\text{trial}}(t)$  was an actual signal recorded from the patient described above (the signal was different for each trial).

$C_{\text{trial}}$  was a number chosen randomly for each trial between 500 and 1500 from a uniform distribution.

$$X_{\text{trial}}^g(t) = \frac{X'_{\text{trial}}{}^g(t)}{\|X'_{\text{trial}}{}^g(t)\|}$$

with  $X'_{\text{trial}}{}^g(t) = G(t)\text{Fil}_{40-45 \text{ Hz}}(X_{\text{trial}})$ .

$G(t)$  was a function that is zero everywhere except on the window  $[1500-2500 \text{ ms}]$  where it was a bell curve going from 0 to 1 then back to 0.

$\text{Fil}_{40-45 \text{ Hz}}(X_{\text{trial}})$  is signal  $X_{\text{trial}}(t)$  bandpass-filtered between 40 and 45 Hz.

$$X_{\text{trial}}^b(t) = \frac{X'_{\text{trial}}{}^b(t)}{\|X'_{\text{trial}}{}^b(t)\|}$$

with  $X'_{\text{trial}}{}^b(t) = B(t)\text{Fil}_{20-25 \text{ Hz}}(X_{\text{trial}})$ .

$B(t)$  was a function that is zero everywhere except on the window  $[0-1000 \text{ ms}]$  where it was a bell curve going from 0 to 1 then back to 0.

$\text{Fil}_{20-25 \text{ Hz}}(X_{\text{trial}})$  was signal  $X_{\text{trial}}(t)$  bandpass-filtered between 20 and 25 Hz.

## References

- Auger F, Flandrin P, Gonzalves P, Lemoine O. Time–frequency toolbox. For use with Matlab Tutorial 1997. Available at <http://www.physique.ens-lyon.fr/ts/tftb.html>.
- Basar E, Basar-Eroglu C, Karakas S, Schurmann M. Brain oscillations in perception and memory. *Int J Psychophysiol* 2000;35(2–3):95–124.
- Bressler S. Annual Meeting of the Society of Biological Psychiatry, Philadelphia, PA, 2002.
- Fries P, Reynolds J, Rorie A, Desimone R. Modulation of oscillatory neuronal synchronization by selective visual attention. *Science* 2001;291(5508):1560–3.
- Friston K. Another neural code? *Neuroimage* 1997;5:213–20.
- Friston K. The labile brain. I. Neuronal transients and nonlinear coupling. *Philos Trans R Soc Lond B* 2000;355:215–36.

- Gardner W. A unifying view of coherence in signal processing. *Signal Process* 1992;29(2):113–40.
- Halgren E, Boujon C, Clarke J, Wang C, Chauvel P. Rapid distributed fronto-parieto-occipital processing stages during working memory in humans. *Cereb Cortex* 2002;12:710–28.
- Hirai N, Uchida S, Maehara T, Okubo Y, Shimizu H. Beta-1 (10–20 Hz) cortical oscillations observed in the human medial temporal lobe. *Neuroreport* 1999;10(14):3055–9.
- Kahana MJ, Sekuler R, Caplan JB, Kirschen M, Madsen JR. Human theta oscillations exhibit task dependence during virtual maze navigation. *Nature* 1999;399(6738):781–4.
- Lachaux JP, Rodriguez E, Martinerie J, Varela F. Measuring phase-synchrony in brain signals. *Hum Brain Mapp* 1999;8(4):194–208.
- Lachaux JP, Rodriguez E, Le Van Quyen M, Lutz A, Martinerie J, Varela F. Studying single-trials of phase-synchronous activity in the brain. *Int J Bifurcat Chaos* 2000a;10(10):2429–39.
- Lachaux JP, Rodriguez E, Martinerie J, Adam C, Hasboun D, Varela F. A quantitative study of gamma-band activity in human intracranial recordings triggered by visual stimuli. *Eur J Neurosci* 2000b;12:2608–22.
- Lachaux JP, Lutz A, Rudrauf D, Cosmelli D, Le Van Quyen M, Martinerie J, Varela F. Estimating the time-course of coherence between single-trial brain signals: an introduction to wavelet-coherence. *Neurophysiol Clin/Clin Neurophysiol* 2002;32:157–74.
- Lutz A, Lachaux JP, Martinerie J, Varela FJ. Guiding the study of brain dynamics by using first-person data: synchrony patterns correlate with ongoing conscious states during a simple visual task. *Proc Natl Acad Sci USA* 2002;99(3):1586–91.
- Miltner W, Braun C, Arnold M, Witte H, Taub E. Coherence of gamma-band EEG activity as a basis for associative learning. *Nature* 1999;397:434–6.
- Raghavachari S, Kahana MJ, Rizzuto DS, Caplan JB, Kirschen MP, Bourgeois B, Madsen JR, Lisman JE. Gating of human theta oscillations by a working memory task. *J Neurosci* 2001;21(9):3175–83.
- Rodriguez E, George N, Lachaux JP, Martinerie J, Renault B, Varela F. Perception's shadow: long-distance synchronization of human brain activity. *Nature* 1999;397:430–3.
- Schanze T, Eckhorn R. Phase correlation among rhythms present at different frequencies: spectral methods, application to microelectrode recordings from visual cortex and functional implications. *Int J Psychophysiol* 1997;26(1–3):171–89.
- Tallon-Baudry C, Bertrand O. Oscillatory gamma activity in humans and its role in object representation. *Trends Cogn Sci* 1999;3:151–62.
- Tallon-Baudry C, Bertrand O, Fischer C. Oscillatory synchrony between human extrastriate areas during visual short-term memory maintenance. *J Neurosci* 2001;21(20):C177.
- Tass P, Rosenblum M, Weule J, Kurths J, Pikovsky A, Volkman J, Schnitzler A, Freund H. Detection of  $n:m$  phase locking from noisy data: application to magnetoencephalography. *Phys Rev Lett* 1998;81:3291–4.
- Varela F, Lachaux JP, Rodriguez E, Martinerie J. The brainweb: phase synchronization and large-scale integration. *Nat Rev Neurosci* 2001;2(4):229–39.
- Von Stein A, Chiang C, Konig P. Top-down processing mediated by interareal synchronization. *PNAS* 2000;97(26):14748–53.